Volume 37 | Issues 5–6 | 2016
Included in this print edition:
Issue 5 (February 15, 2016)
Issue 6 (March 5, 2016)

Journal of COMPUTATIONAL CHEMISTRY

Organic • Inorganic • Physical
Biological • Materials

www.c-chem.org

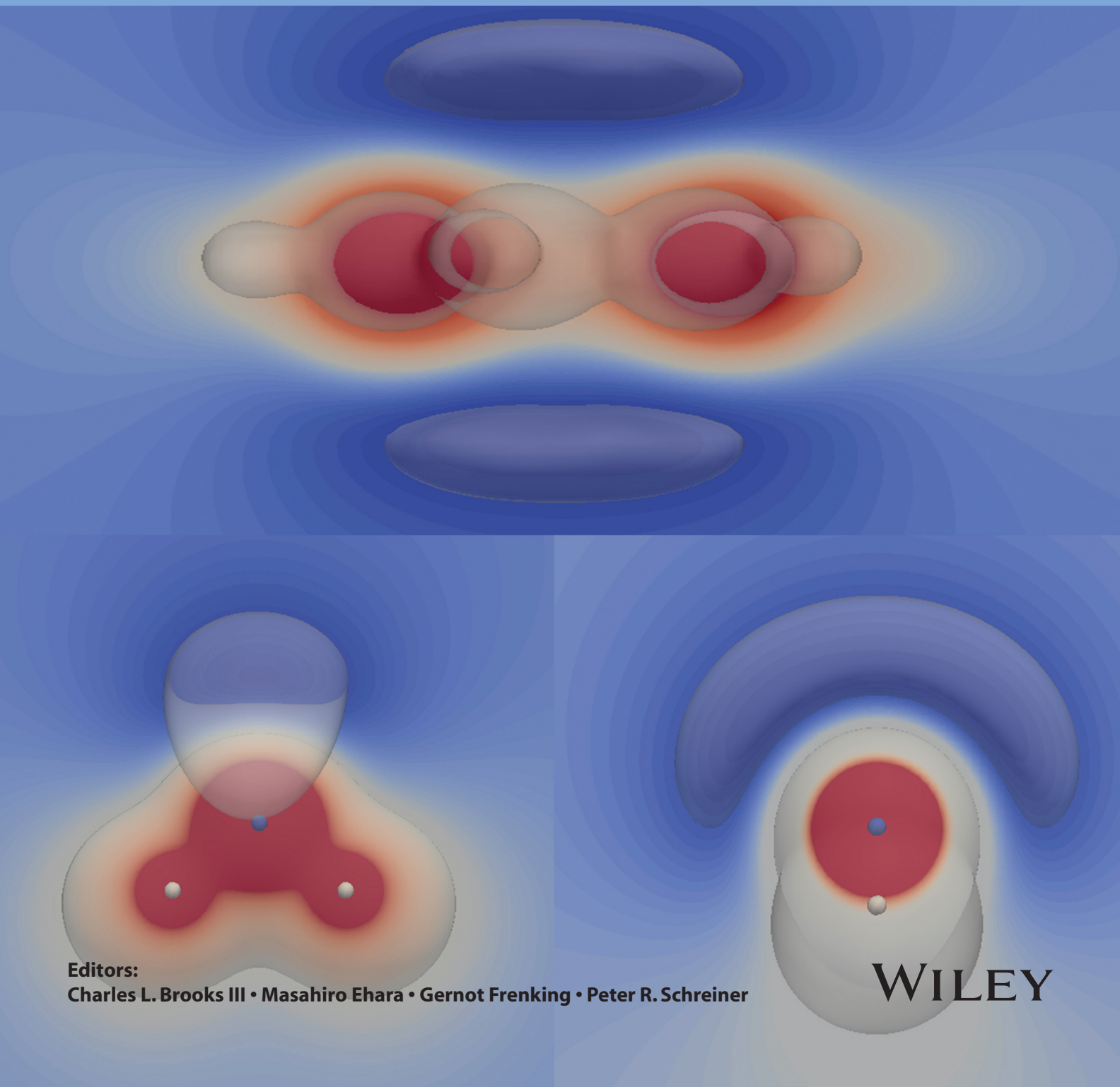

Editors:
Charles L. Brooks III • Masahiro Ehara • Gernot Frenking • Peter R. Schreiner

WILEY

Scalable Improvement of SPME Multipolar Electrostatics in Anisotropic Polarizable Molecular Mechanics Using a General Short-Range Penetration Correction up to Quadrupoles

Christophe Narth,[a] Louis Lagardère,[b] Étienne Polack,[a,c] Nohad Gresh,[a,d] Qiantao Wang,[e] David R. Bell,[e] Joshua A. Rackers,[f] Jay W. Ponder,[g] Pengyu Y. Ren,*[e] and Jean-Philip Piquemal*[a]

We propose a general coupling of the Smooth Particle Mesh Ewald SPME approach for distributed multipoles to a short-range charge penetration correction modifying the charge-charge, charge-dipole and charge-quadrupole energies. Such an approach significantly improves electrostatics when compared to *ab initio* values and has been calibrated on Symmetry-Adapted Perturbation Theory reference data. Various neutral molecular dimers have been tested and results on the complexes of mono- and divalent cations with a water ligand are also provided. Transferability of the correction is adressed in the context of the implementation of the AMOEBA and SIBFA polarizable force fields in the TINKER-HP software. As the choices of the multipolar distribution are discussed, conclusions are drawn for the future penetration-corrected polarizable force fields highlighting the mandatory need of non-spurious procedures for the obtention of well balanced and physically meaningful distributed moments. Finally, scalability and parallelism of the short-range corrected SPME approach are addressed, demonstrating that the damping function is computationally affordable and accurate for molecular dynamics simulations of complex bio- or bioinorganic systems in periodic boundary conditions. © 2016 Wiley Periodicals, Inc.

DOI: 10.1002/jcc.24257

Introduction

The field of molecular modeling is growing exponentially. The increase of available crystallographic structures[1–3] over the years has posed a substantial challenge for molecular force field development. For such systems, classical approaches still encounter successes but also reach their limits when describing nonbonded interactions, which can only be reliably computed using quantum chemistry. Year after year, it becomes clear that the gap between quantum and classical approaches is too wide to be ignored, should one attempt to be predictive. First-generation force fields ignore polarization effects and employ a simple electrostatic term while a van der Waals interaction term takes the role of a buffer contribution including all quantum-like effects. To compute interaction energies of high accuracy that could be compared directly to quantum chemistry and/or experiments, one should build force fields that embody all anisotropic effects and are able to separately reproduce all quantum contributions. Among all terms, electrostatics remains prominent.[4,5] Point charges can appropriately capture some long-range electrostatics but, quantum chemistry clearly shows the need to go beyond such an approximation to handle anisotropic interactions. Usually, distributed multipoles are used to account for polarization, but they are devoid of the short-range electrostatic quantum effects, the so-called charge penetration, which occurs when the molecular densities overlap. Various strategies have been employed to include such effects. They range from damping functions[6,7] to neural networks[8] and

[a] *C. Narth, É. Polack, N. Gresh, J.-P. Piquemal*
UPMC Univ. Paris 06, UMR 7616, Laboratoire de Chimie Théorique, F-75005 Paris, France
E-mail: jpp@lct.jussieu.fr
[b] *L. Lagardère*
UPMC Univ. Paris 06, Institut du Calcul et de la Simulation, F-75005 Paris, France
[c] *É. Polack*
UPMC Univ. Paris 06, UMR 7598, Laboratoire Jacques-Louis Lions, F-75005 Paris, France
[d] *N. Gresh*
Chemistry and Biology Nucleo(s)tides and immunology for Therapy (CBNIT), UMR 8601 CNRS, UFR Biomédicale, Paris, 75006 France
[e] *Q. Wang, D. R. Bell, P. Y. Ren*
Department of Biomedical Engineering, The University of Texas at Austin, Texas 78712
E-mail: pren@mail.utexas.edu
[f] *J. A. Rackers*
Computational and Molecular Biophysics Program, Washington University, St. Louis, Missouri, 63110
[g] *J. W. Ponder*
Department of Chemistry, Washington University in St. Louis, St. Louis, Missouri, 63130

Contract grant sponsor: CALSIMLAB and the ANR; Contract grant number: ANR-11-idex-0004-02; Contract grant sponsor: Robert A. Welch Foundation; Contract grant number: F-1691; Contract grant sponsor: National Institutes of Health; Contract grant number: gm106137 and GM 114237 to J.W.P., P.R., J.P.P.; Contract grant sponsor: TACC and XSEDE; Contract grant number: tg-mcb100057; Contract grant sponsor: French CNRS through PICS grant; Contract grant sponsor: Délégation Générale de l'Armement (DGA); Contract grant sponsor: Maîtrise NRBC; Contract grant sponsor: from the French Ministry of Defense; Contract grant sponsor: National Science Foundation; Contract grant number: CHE1152823 to J.W.P.

© 2016 Wiley Periodicals, Inc.

to newly developed point-distributed electron densities such as the GEM[9,10] potential. Quantum mechanical (QM) force fields[11] also address this topic. Clearly, both short- and long-range electrostatics do matter and one would like to treat them in concert. This was done in the context of GEM that uses continuous electrostatics, which resort to electron densities. To do so, a generalized Smooth Particle Mesh Ewald (SPME) approach was introduced which handles Hermite Gaussians thereby including penetration effects. As shown initially by Darden et al.,[12,13] the PME and SPME strategies provide a scaling improvement enabling to deal with electrostatics in periodic boundary conditions with a $N \log(N)$ complexity as compared to the usual direct space N^2. In this contribution, we propose a simple strategy based on a damping function to include short-range penetration within a distributed multipole SPME framework. Its aim is to be applicable to modern polarizable molecular dynamics (MD) using force fields such as AMOEBA[14] and Sum of Interactions Between Fragments *Ab-initio* computed (SIBFA).[7,15–19] The article is organized as follows. We first present our choice of charge penetration correction. We then briefly recall the SPME methodology for distributed multipoles before presenting a newly developed coupled approach. Finally, we present the parametrization procedure, the numerical results, and a parallel implementation.

Charge Penetration

The question of the atomic charge description has previously been investigated.[7,9,20–25] In classical force fields, the charge distribution is modeled using point charges calibrated on the Molecular Electrostatic Potential (MEP) computed with QM methods.[26] Although the anisotropy, is not directly taken into account even in the case of MEP fitting,[27,28] this method is still widely used among various communities as it allows the simulation of very large systems due to its low computational cost.

The Distributed Multipole Analysis[29] (DMA) has been shown to be a suitable description of the charge distribution to improve electrostatics. Other distributed multipole methods exist. For example, one of the first full-fledged polarizable force fields, SIBFA,[7,15–18] originally used the multipole partitioning scheme developed by Vigné-Maeder and Claverie.[30,31] Nevertheless, none of these multipole methods properly account for the overlap of molecular densities at short-range. In physical systems, this overlap gives rise to a mainly attractive energy denoted electrostatic penetration. Hence, distributed multipoles cannot be rigorously accurate at all ranges because of their classical approximation of electrostatics: they cannot describe the purely QM charge penetration effect.

From quantum intermolecular perturbation theory, one can see that charge penetration exhibits an exponential decay being density overlap-dependent.[31,32]

Charge penetration has been widely studied in QM. For example, Jeziorski et al. studied Helium dimer intermolecular potential to find a classical description of its potential by means of Energy Decomposition Analysis, here Symmetry Adapted Perturbation Theory[33,34] (SAPT).

We extended this SAPT study to Neon and Argon dimers. Figure 1 exhibits the electrostatic component for these three rare gas dimers as a function of their interatomic distances. One can notice (i) the existence of a non-zero electrostatic energy component at short-range and (ii) the confirmation of the exponential decay. This observation and the fact that the rare gas charge is zero, and therefore does not have any classical electrostatic contribution, suggests that short-range effects should also be included.

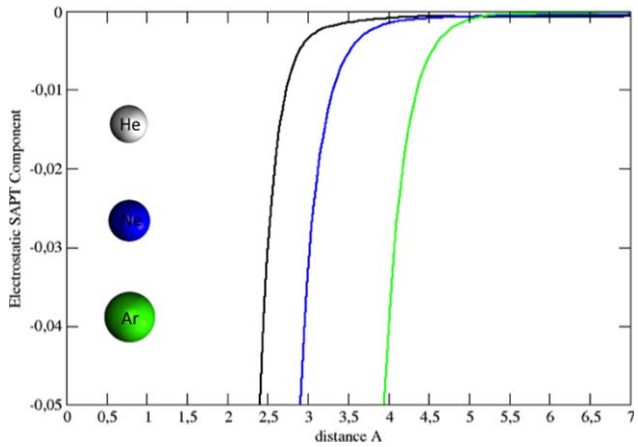

Figure 1. Electrostatics contribution of rare gas dimers in kcal/mol.

In that context, Piquemal et al. have proposed a damping correction[7,18] grounded in Quantum Chemistry (QC) [see eq. (1)]. Indeed, the electrostatic energy between two monomers (A and B) can be expressed as:

$$E_{\text{elec}} = -2\sum_i \sum_\nu Z_\nu \int \frac{|\varphi_i(1)|^2}{r_{i\nu}} dr_1{}^3 - 2\sum_j \sum_\mu Z_\mu \int \frac{|\varphi_j(2)|^2}{r_{j\mu}} dr_2{}^3 + 4\sum_i \sum_j \int \frac{|\varphi_i(1)|^2 |\varphi_j(2)|^2}{r_{12}} dr_1{}^3 dr_2{}^3 + \sum_\mu \sum_\nu \frac{Z_\mu Z_\nu}{r_{\mu\nu}} \quad (1)$$

where μ (ν) and φ_i (φ_j) are, respectively, the nucleus and the unperturbed molecular orbitals of monomer A (B) and Z is the atomic number. The first two terms define nucleus-electron attraction, the third the electron-electron repulsion and the fourth the nucleus-nucleus repulsion. This strongly suggests that mimicking such a term is a key ingredient to correctly model all the components of electrostatics. The electronic integrals explain the appearance of electrostatic exponential decay. As charge penetration is missing, it seems reasonable to consider the outer-shell electrons (electronic valence) in the construction of an overlap-based short-range correction. Indeed, as shown in Figure 1 the atomic size is important, and is closely linked to the magnitude of the penetration effect. One would like to consider van der Waals-like radii as a component of the parametrization. In that context,[18] Piquemal et al. proposed a short-range correction to the multipolar electrostatics that includes all these features and was originally implemented in SIBFA. The latter modifies the charge-charge, charge-dipole, and charge-quadrupole interactions.

The aim of this article is to include and to reparametrize this correction in the framework of the SPME. The proposed correction modifies the charge-charge (2) and charge-dipole (3). The latter involves a damped charge that is also appicable

to correct the charge-quadrupole interactions.[18] These three terms are the dominant ones.[7]

$$E^*_{m_i-m_j}=\frac{1}{r_{ij}}[Z_iZ_j-Z_i(Z_j-q_j)(1-\exp(-\alpha_j r_{ij}))$$
$$-Z_j(Z_i-q_i)(1-\exp(-\alpha_i r_{ij}))$$
$$+(Z_i-q_i)(Z_j-q_j)(1-\exp(-\beta_i r_{ij})(1-\exp(-\beta_j r_{ij})] \quad (2)$$

where $\alpha_i=\gamma/r^i_{vdw}$ and $\beta_i=\delta/r^i_{vdw}$, γ and δ are normalization coefficients and r^i_{vdw} the van der Waals radius of atom i. Z_i is the electronic valence of the atom i, q_i the charge (monopole) of atom i.

$$E^*_{m_i-d_j}=\frac{\mu_j.\mathbf{r}_{ji}}{r^3_{ij}}(Z_i-(Z_i-q_i)(1-\exp(-\eta_i r_{ij})) \quad (3)$$

where $\eta_i=\chi/r^i_{vdw}$, with χ a normalization coefficient.

This charge-charge correction contains the traditional coulombic expression, corresponding to nucleus-nucleus repulsion. The formulation considers two more contributions, nucleus-electron attraction and electron-electron repulsion, where the damping function appears. It describes the depletion of the electronic cloud at short-distance. Following the same idea, the charge-dipole also accounts for this depletion by modulating the charge.[20] It is worth mentioning that at long-range, this term tends to the classical coulombic electrostatic expression. In MD, conformational exploration of space can lead to very short-interatomic distances where multipoles clearly fail to recover the QM values due to the lack of charge penetration effect. Usually such errors are compensated by parametrization of the van der Waals terms. However, there is no guarantee of a systematic compensation during such MD simulations, the lack of which could lead to errors. To apply this methodology to large systems and perform MD, we propose to couple this approach to the SPME.[12]

Smooth particle mesh Ewald

SPME is based on the Ewald summation,[35] which suggests to split the electrostatics into two terms, a short-range E_{dir} and a long-range one E_{rec} and whose complexity is N^2 or even $N^{3/2}$.[36] SPME decreases it to $N\log N$ by using Fast Fourier Transforms (FFT).[35]SPME can be applied to condensed phase. In that case, the lower complexity leads to particularly large time savings for large systems in MD. SPME is an efficient and adaptable algorithm, as its formulation for multipoles[37,38] and for the charge penetration correction suggests. In this section, we show how to modify the general SPME formulas in order to include the charge penetration correction.

Let U be a neutral unit cell with N particles in position $(\mathbf{r}_i)_{i\in\{1,\cdots,N\}}$ and respective multipolar moments $(\hat{L}_i)_{i\in\{1,\cdots,N\}}$, $(\mathbf{a}_1,\mathbf{a}_2,\mathbf{a}_3)$ its basis and Σ the system made of an infinite number of images of the unit cell.

For any integers n_1,n_2,n_3,m_1,m_2 and m_3 we will note

$$\mathbf{n}=n_1\mathbf{a}_1+n_2\mathbf{a}_2+n_3\mathbf{a}_3 \quad \mathbf{m}=m_1\mathbf{a}^*_1+m_2\mathbf{a}^*_2+m_3\mathbf{a}^*_3,$$

where $(\mathbf{a}^*_1,\mathbf{a}^*_2,\mathbf{a}^*_3)$ is the dual basis of $(\mathbf{a}_1,\mathbf{a}_2,\mathbf{a}_3)$ (*i.e.* $\mathbf{a}^*_i\cdot\mathbf{a}_j=\delta_{ij}$).

The electrostatic energy of the system is

$$E_{\text{elec}}(\Sigma)=\frac{1}{2}\sum_{\mathbf{n}}{}'\sum_{1\le i,j\le N}\hat{L}_i\hat{L}_j\left(\frac{1}{|\mathbf{r}_j-\mathbf{r}_i+\mathbf{n}|}\right), \quad (4)$$

where the prime means that the terms $i=j$ are not summed up when $\mathbf{n}=0$. If we consider multipoles up to quadrupoles, then the operators $\hat{L}_i$ can be written as

$$\hat{L}_i(\mathbf{m})=q_i+\boldsymbol{\mu}_i\cdot\nabla_i+Q_i:\nabla_i\nabla_i, \quad (5)$$

where ∇_i is the gradient at $\mathbf{r}_i$, $\boldsymbol{\mu}$ and $\boldsymbol{Q}$ are the dipoles and the quadrupole moments.

For any $\mathbf{m}\in\mathbb{R}^3$ we define the structure factor

$$S(\mathbf{m})=\sum_j\tilde{L}_j(\mathbf{m})\exp(2\pi\mathbf{m}\cdot\mathbf{r}_j) \quad (6)$$

where $\tilde{L}_j$ is the Fourier transform of the operator $\hat{L}_j$, *i.e.*

$$\tilde{L}_j=q_j+2i\pi\ \boldsymbol{\mu}_j\cdot\mathbf{m}-(2\pi)^2Q_j:\mathbf{mm}, \quad (7)$$

If Σ is supposed to be surrounded by a medium with infinite dielectric constant, then it has been shown that for any $\beta>0$ the sum can be split as[38]

$$E_{\text{elec}}(\Sigma)=E_{\text{dir}}+E_{\text{self}}+E_{\text{rec}}, \quad (8)$$

where

$$E_{\text{dir}}=\sum_{\mathbf{n}}{}'\sum_{1\le i,j\le N}\hat{L}_i\hat{L}_j\left(\frac{\text{erfc}(\beta|\mathbf{r}_j-\mathbf{r}_i+\mathbf{n}|)}{|\mathbf{r}_j-\mathbf{r}_i+\mathbf{n}|}\right), \quad (9)$$

$$E_{\text{self}}=-\frac{\beta}{\sqrt{\pi}}\sum_{j=1}^{N}\left(q_j^2+\frac{2\beta^2}{3}\left(\boldsymbol{\mu}_j^2-2q_j\text{Tr}(Q_j)\right)+\frac{4\beta^4}{5}\left(2Q_j:Q_j+\text{Tr}^2(Q_j)\right)\right), \quad (10)$$

and (11)

$$E_{\text{rec}}=\frac{1}{2\pi V}\sum_{\mathbf{m}\neq 0}\frac{\exp(-\pi^2\mathbf{m}^2/\beta^2)}{\mathbf{m}^2}S(\mathbf{m})S(-\mathbf{m}). \quad (12)$$

The self energy term[39] E_{self} is a bias due to the Ewald summation and does not have any physical meaning. Both the direct and the reciprocal sums converge rapidly. A 9 Å cutoff is common, allowing a $O(N)$ computational complexity for the direct sum. The B-spline approximation of the structure factor on a grid of dimensions $K_1\times K_2\times K_3$ enables the reciprocal energy to be approximated by

$$\tilde{E}_{\text{rec}}=\frac{1}{2}\sum_{k_1=0}^{K_1-1}\sum_{k_2=0}^{K_2-1}\sum_{k_3=0}^{K_3-1}Q(k_1,k_2,k_3)\cdot(\theta_{\text{rec}}*Q)(k_1,k_2,k_3), \quad (13)$$

where Q is a derivable function obtained after interpolation of the structure factors at the nodes of the grid; and θ_{rec} a pair-potential function independent of particle position. The regularity of Q implies that the force in position i can be approximated by

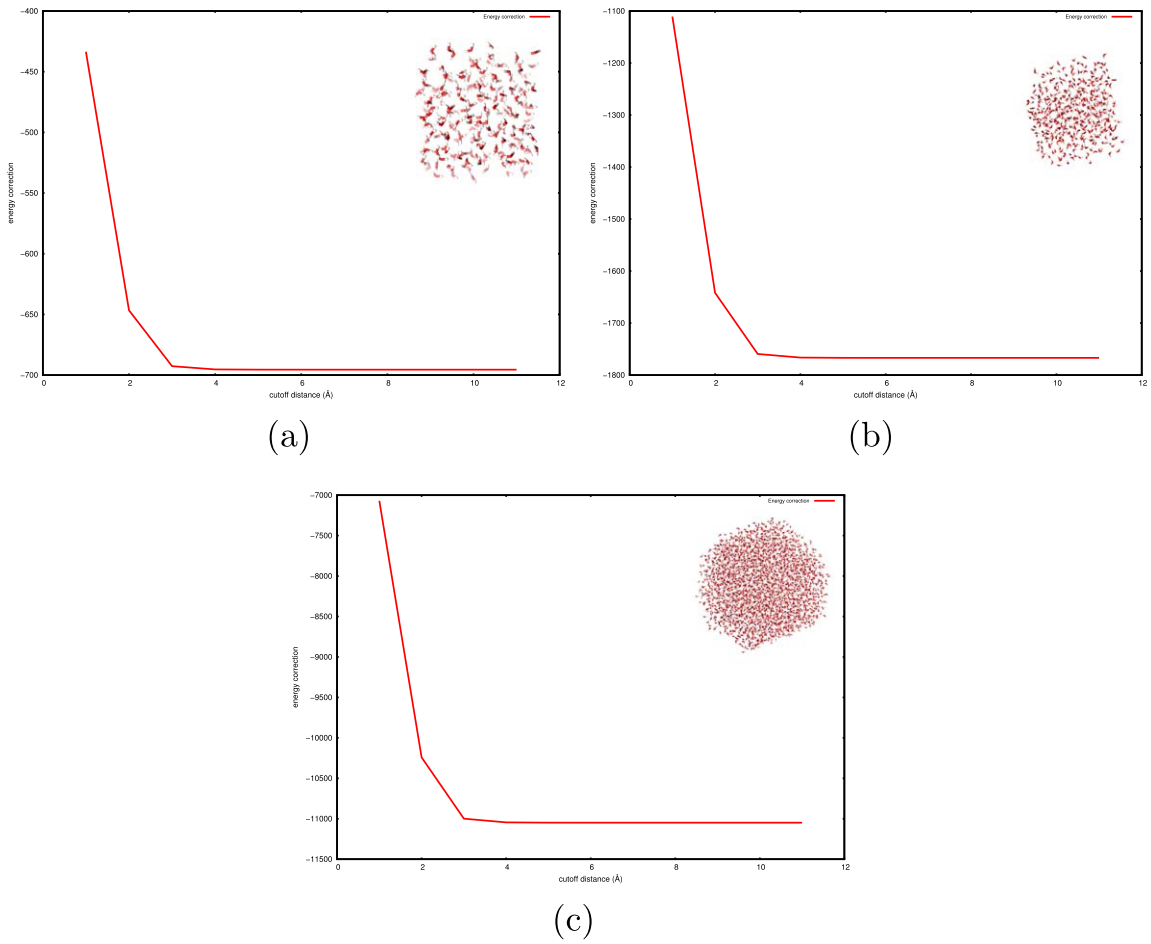

Figure 2. Convergence cutoff study of penetration energy. Energy in kcal/mol.

$$\tilde{\mathbf{F}}_i = -\nabla_i \tilde{E}_r = \frac{1}{2}\sum_{k_1=0}^{K_1-1}\sum_{k_2=0}^{K_2-1}\sum_{k_3=0}^{K_3-1} \nabla_i Q(k_1,k_2,k_3)\cdot(\theta_{\text{rec}} * Q)(k_1,k_2,k_3). \tag{14}$$

In principle, the short-range correction is only in the direct space and therefore we will show that no modification of the reciprocal sum is required. We will detail our strategy of implementation aimed at an optimal scalability of the corrected electrostatics. As we discussed, the presented implementation in SPME requires a modification of the direct sum only. To do so, we need to reexpress the damping function by Piquemal et al. in more convenient form as a simple correction to the direct sum.

Coupling SPME and a penetration correction

Let us define E^*_{elec} the total modified/damped electrostatic energy of the system Σ.

$$E^*_{\text{elec}}(\Sigma) = \frac{1}{2}\sum_{\mathbf{n}}{}' \sum_{1\le i,j\le N} E^*_{m_i-m_j} + E^*_{m_i-d_j} + E^*_{m_i-q_j} + E_{d_i-d_j} + E_{d_i-q_j} + E_{q_i-q_j} \tag{15}$$

where $E_{d_i-d_j}$ is the interaction between dipoles of site i and site j; $E_{m_i-q_j}$, $E_{d_i-q_j}$ and $E_{q_i-q_j}$ are respectively the interaction between monopole/dipole/quadrupole of site i and quadrupole of site j. Let us define E_{pen} the total charge penetration energy,

$$E_{pen} = E^*_{\text{elec}} - E_{\text{elec}} = \sum_{\mathbf{n}}{}' \sum_{1\le i,j\le N} E^*_{m_i-m_j} - E_{m_i-m_j} + E^*_{m_i-d_j} - E_{m_i-d_j} \tag{16}$$

Let us define the undamped electrostatic interaction between the monopoles of sites i and j $E_{m_i-m_j}$, let us also define the undamped electrostatic interaction between the dipole of site j and the monopole of site i $E_{m_i-d_j}$.

$$\begin{aligned} E^*_{m_i-m_j} - E_{m_i-m_j} &= (q_i-Z_i)(q_i-Z_j)(\exp(-\beta_i r_{ij})-1)(\exp(-\beta_j r_{ij})-1) \\ &-(q_j-Z_i)Z_j(\exp(-\alpha_i r_{ij})-1)-(q_i-Z_j)Z_i(\exp(-\alpha_j r_{ij})-1)-q_iq_j+Z_iZ_j \end{aligned} \tag{17}$$

$$E^*_{m_i-d_j} - E_{m_i-d_j} = \frac{\mu_j \cdot \mathbf{r}_{ji}}{r_{ij}^3}(Z_i-q_i)\exp(-\eta r_{ij}) \tag{18}$$

$$E^*_{\text{elec}} = E_{\text{elec}} + E_{pen} \tag{19}$$

The same strategy has been followed to correct the charge-quadrupole interaction.[18]

As seen in section "Smooth Particle Mesh Ewald," E_{pen} cannot be simply included into the SPME framework, as we should take a large cutoff for the direct sum to avoid any persistence of penetration outside the direct sum treatment.

Indeed, the charge penetration energy is prominent at short-range and tends quickly to zero at long-range because of its $\exp(-x)/x^n$ (with $n = 1, 3$) form (see Fig. 4) but not necessarily fast enough to be maintained within the Ewald direct sum cutoff. Because, however, resorting to cutoffs generates discontinuity and non-derivability of the potential function near the cutoff limit, we will couple them to a switching function ensuring derivability in the course of an entire MD simulation. As such an approach generates a discontinuity and non-derivability in the potential function near the cutoff limit. We will couple it with a switching function that ensures derivability of the energy during an MD simulation. Many smoothing functions have been proposed[40] and we chose to use the one defined in Refs. [41] and [42] [eq. (20)]. Hence, for every distance r, the potential energy is equal to $V(r) \cdot S(r)$ where $V(r)$ is the unswitched function. The interactions are not modified for distances less than an inner cutoff distance R_{in} and are smoothed to zero at the outer cutoff R_{out}. Besides, the continuity of the first derivatives prevents jumps in the energy during MD or minimization, which could lead to nonphysical phenomena such as heating.

Such a technique enables to keep the long-range effects and the computational advantage of SPME using FFTs with an optimal Ewald cutoff, while just adding a computationally cheap correction term with its own cutoff (see Fig. 2). Besides, numerical simulations of common systems (up to tens of thousands of atoms) show that a cutoff between 6 and 8 Å guarantees an error inferior to 10^{-3} kcal/mol (see Fig. 2). Of course, the smoothing function makes possible to choose a more aggressive cutoff of 4 Å (see Fig. 2) which will capture most of the penetration interaction in common systems leading to significant computational speed-up. Overall, the final cost in term of computational ressources of the penetration correction is inferior to 10% of the total penetration corrected multipolar electrostatics.

$$S(r) = \begin{cases} 1 & r \le R_{\text{in}} \\ \dfrac{(R_{\text{out}}^2 - r^2)^2 (R_{\text{out}}^2 + 2r^2 - 3R_{\text{in}}^2)}{(R_{\text{out}}^2 - R_{\text{in}}^2)^3} & R_{\text{in}} < r \le R_{\text{out}} \\ 0 & r > R_{\text{out}} \end{cases} \quad (20)$$

Results

Parametrization

The electrostatic correction includes four empirical parameters: two for charge-charge interactions (core-electron attraction and electron-electron repulsion), one for charge-dipole interactions, and one for charge-quadrupole. Those were initially adjusted on water dimers.[43–46] As various parametrization strategies are possible, the atomic radius can be used as a parameters in order to reproduce the charge penetration effect. This is applied to various choices of distributed multipoles. We focused on the GDMA approach by Stone[29] and on the electrostatic potential (ESP)[14] fitted multipoles used in the AMOEBA force field. We first follow the initial parametrization strategy developed for SIBFA and then we choose a simpler exponential functional form for the parametrization that does not take into account any atom radii. In this form, the parameters are the previously defined exponents:[18] α_i, β_i, and η_i.

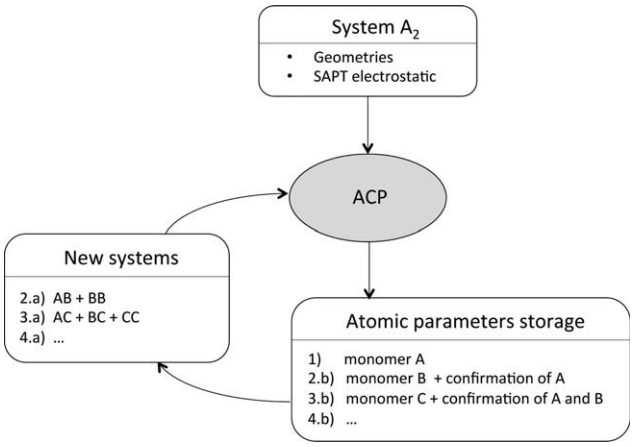

Figure 3. Flowchart Automated Calibration Procedure (ACP).

We focused our parametrization on a well established panel of intermolecular systems extracted from the S66 dataset as well as on selected configurations of water dimers obtained from high level *ab-initio* computation.[44,47,48] Several QM intermolecular energy decomposition techniques are now available such as reduced variational space[49] or SAPT.[34] SAPT offers the possibility to include all types of intermolecular interactions, as it allows to take into account electronic correlation. Because our upcoming implementation should reproduce all of them in an advanced quantum chemistry-grounded polarizable force-field, we chose to calibrate the electrostatics on SAPT. Note that the idea is to reproduce electrostatic trends at all ranges, with a special focus at short-ranges where charge penetration matters, which could make a perfect match with QM reference values difficult.

The first step of our calibration was to find the best set of parameters for ten different water dimers associated to stationary points on the *ab-initio* potential energy surface (denoted A on Fig. 3). Four of these dimers were chosen (see Fig. 4) to refine our results because they represent different chemical situations. Next, a new dimer (denoted B on Fig. 3) as well as monomer-water systems (step 2 on Fig. 3) can be calibrated. Thus, new parameters can be tested on dimers involving noncalibrated monomers (denoted C on Fig. 3). This also allows to validate the previous calibration.

Each system was considered at its lower energy value configuration and at different intermolecular distances. These kinds of variation are likely to happen in MD and accounting for them will make our model more robust, as it would be able to sample density overlapping regions.

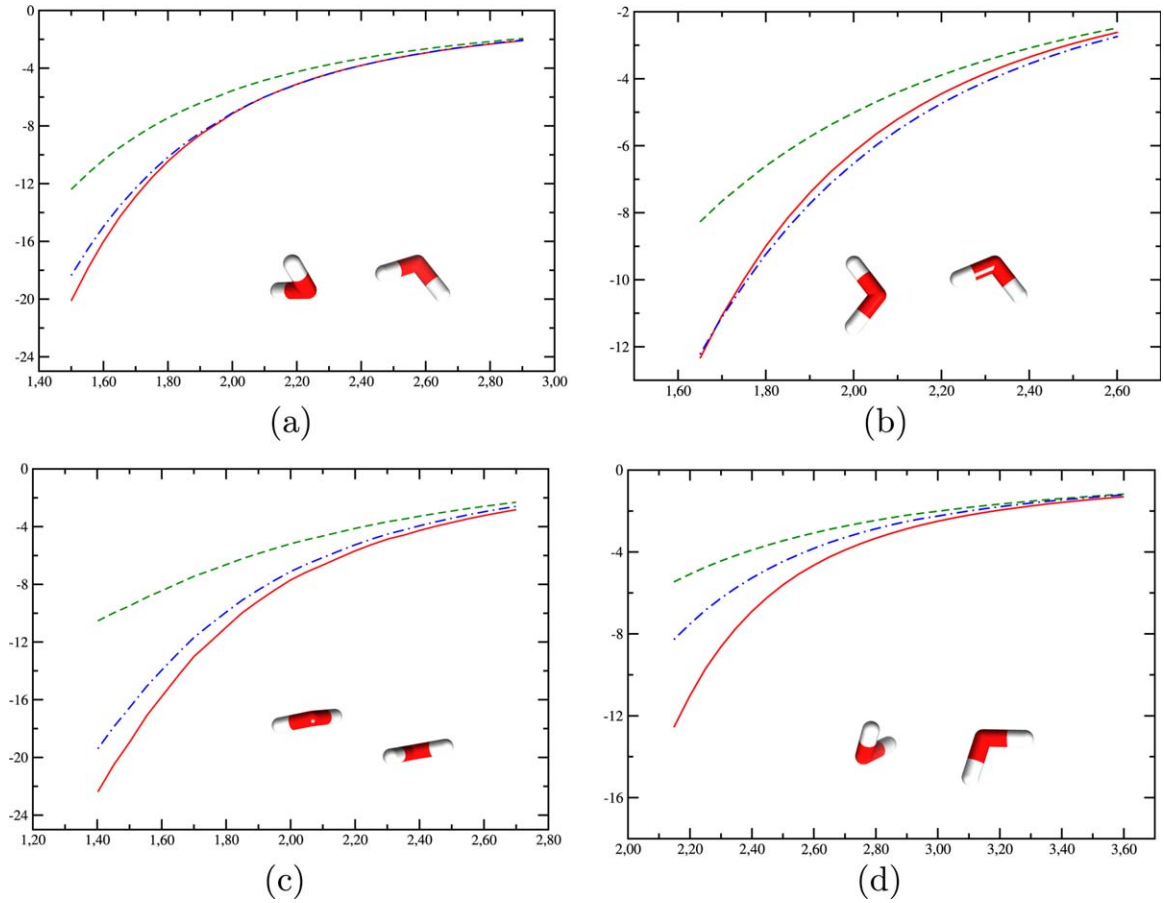

Figure 4. Water dimers electrostatic profile as function of intermolecular distance in kcal/mol. SAPT is the red line. AMOEBA the green dashed line. CP-AMOEBA the blue dashed dot line. [Color figure can be viewed in the online issue, which is available at wileyonlinelibrary.com.]

Computational details

The parallel implementation was first tested on the SGI UV 2000 supercomputer of the ICS (Institut du Calcul et de la Simulation) which is made of 64 nodes each having two Intel Xeon E5-4650L CPUs with eight cores at 2.6 Ghz and 256 GB of DDR3 DIMM RAM. The nodes are able to communicate within a global shared memory system thanks to the SGI NUMALINK interconnect. We also tested our MPI implementation on the Stampede supercomputer of the TACC (Texas Advanced Computing Center) whose architecture is more standard as it consists, for the part we did our tests on, of 6400 compute nodes with two intel Xeon E5-2680 CPUs with eight cores at 2.7Ghz, one Intel Xeon Phi SE10P coprocessor and 32 GB of DDR3 DIMM RAM. These nodes communicate within a 56 GB/s InfiniBand network. The following numerical results are all based on computations made on this supercomputer. SAPT calculations have been performed using PSI4[50] at third order for water dimers and at second order for the other complexes. All GDMA multipoles were computed from density at the MP2/aug-cc-pVTZ.

Numerical results

Tables 1 and 2 gather various results for ten selected orientation of the water dimer[44] including pure multipolar interactions (Table 1) and damped multipolar ones (Table 2). Such configurations are clearly difficult as they embody various types of orientations involving very different anisotropic orbital interactions. Columns 2 to 4 of Table 1 describe the values of the GDMA, atoms and bond midpoints then atoms only and ESP fitted multipoles energies. In the first approximation, compared with reference SAPT and to atoms only GDMA multipoles, one would think that having more centers improves electrostatics. Overall, the ESP fit appears to improve the agreement with the SAPT

Table 1. Comparison of the pure multipolar electrostatics to SAPT Coulomb energy in then water dimers (values in kcal/mol).

Index	$GDMA^2$	$GDMA^1$	ESP	SAPT
1	−6.91	−6.73	−6.04	−7.96
2	−5.22	−5.15	−5.28	−6.72
3	−4.88	−4.85	−5.22	−6.52
4	−4.72	−4.82	−4.63	−6.61
5	−3.55	−3.76	−4.26	−5.71
6	−3.19	−3.44	−4.20	−5.41
7	−3.52	−3.58	−3.15	−4.84
8	−1.28	−1.26	−0.94	−1.49
9	−3.87	−3.79	−3.15	−4.71
10	−2.24	−2.21	−2.03	−2.71

$GDMA^i$ describes the multipolar sites scheme, $i = 1$ atoms only and $i = 2$ atoms and bonds.

Table 2. Comparison of the penetration corrected electrostatics to SAPT Coulomb energy in then water dimers (values in kcal/mol).

Index	CP-GDMA^2	CP-GDMA^1	CP-ESP	Ref. 25	SAPT
1	−8.96	−8.18	−7.87	−6.9	−7.96
2	−7.32	−6.64	−6.94	−6.3	−6.72
3	−7.03	−6.36	−6.86	−6.5	−6.52
4	−6.48	−6.58	−6.10	−6.3	−6.61
5	−5.61	−5.78	−5.65	−6.0	−5.71
6	−5.40	−5.58	−5.56	−6.2	−5.41
7	−4.38	−4.71	−3.96	−4.5	−4.84
8	−1.20	−1.43	−1.19	−1.1	−1.49
9	−5.02	−4.84	−3.90	−4.9	−4.71
10	−2.87	−2.82	−2.48	−3.6	−2.71

GDMA^i describes the multipolar sites scheme, $i = 1$ atoms only and $i = 2$ atoms and bonds.

results. The addition of more centers has been already described in the literature by Claverie and Stone[16,29] as a means to capture higher order effects, atoms plus bond midpoints being equivalent to the addition of octupoles within a distributed multipole analysis. Such an observation might need, however, to be reconsidered. Indeed, the derivation of multipoles is usually said to be non-empirical, however, choices exist within the GDMA algorithm including the choice of the partition approach, the choices of the hydrogen radius, etc. Here we tried various settings and kept the following values for the GDMA approach (space partitioning: switching 2, Hydrogen radius 0,325 Å). Choices also exist for the ESP-fitted multipoles as, within the procedure, the charge is initially derived from GDMA and is kept frozen whereas dipole and quadrupole moments are reoptimized to minimize the differences with respect to the *ab initio* electrostatic potential. Overall, with all possible choices, a continuum of multipole sets can be derived with strong energetical differences. Which set should be chosen and are the ESP-fitted parameters indeed better? The application of the damping function to distributed multipoles casts a new light on such an issue. Clearly, the atoms plus bond midpoints GDMA and ESP-fitted multipoles corrected results (see Table 2) are improved by damping but surprisingly the best agreement is found for the damping of atoms only GDMA multipoles. A clear-cut explanation can be found by a careful analysis of the multipolar values alone (Table 1) compared with SAPT. Both GDMA (atoms plus midpoints) and ESP multipoles energies are too high. Indeed, even, with the best choice of settings, some GDMA

Table 3. rmse for distance scans of water dimers (see text) values in kcal/mol (reference SAPT).

Water dimer	CP-AMOEBA	AMOEBA
1	0.51	2.81
3	0.25	1.66
4	1.22	4.86
7	1.39	1.88
S66	0.69	2,21

Table 4. Absolute best timings (in seconds) and number of cores used (in parentheses) for the computation of the electrostatic forces with SPME and of the correction in our implementation.

	Pure MPI	Hybrid OpenMP/MPI
SPME	0.070 (256)	0.040 (512)
CP-AMOEBA	0.025 (256)	0.015 (512)

configuration energies are almost equal to the full quantum SAPT energies that embody penetration and therefore that should be larger. In a sense, the apparently good behavior of the multipolar energies is artificial and is a consequence of a spurious fit that only minimizes the ESP potential without providing an adequate physical picture of the distribution of moments on centers. It is of course, exacerbated by the use of damping functions that add another correction to GDMA analysis. In other words, if the multipolar energy of a given configuration is, by chance, spuriously correct, the damping correction will only destroy the fictitious agreement. For large basis sets, the advantage of having a larger number of centers tend to generate lower quality distributed multipoles because of the difficult handling of diffuse function.[29] Damping indeed requires physically meaningful multipoles with a consistent representation of the different angular momenta. For ESP fitted multipoles, no charge redistribution is provided for the reoptimization of the dipole and quadrupole moments. It generates a better fit for some configurations but also partially reduces anisotropy. Indeed, moments are related to atomic orbital symmetries. If one component is overfitted, the others are clearly less accurately or spuriously described. Overall, whatever the strategy to parametrize the damping function, one has to start to analyze the multipolar energy behavior compared with SAPT: both sets of energies should be clearly different as multipoles do not embody penetration energy. Any attempt to damp overfitted energies will lead to a loss of accuracy when damping is added, especially if one studies various anisotropic interactions. If well-

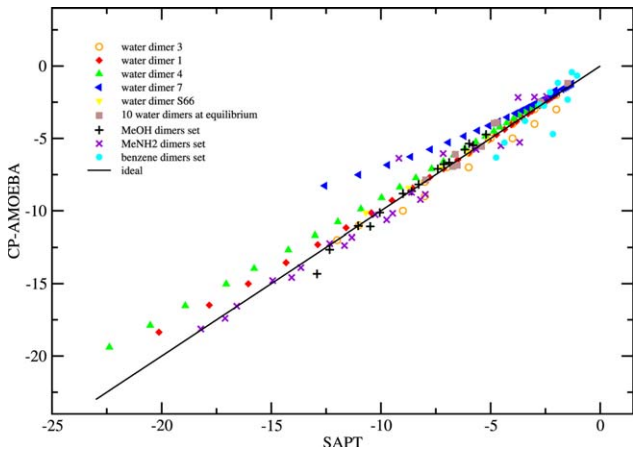

Figure 5. Correlation between SAPT and the penetration correction in kcal/mol within binding range for various dimers (see legend). [Color figure can be viewed in the online issue, which is available at wileyonlinelibrary.com.]

balanced multipoles are extracted, the damping is then increasingly effective as the order of correction tends toward charge-quadrupole (see Appendix). If overfitted multipoles are chosen, one can still strongly reduce the error with SAPT but a charge-charge correction should be prefered as higher-order corrections will be perturbed by the spurious anisotropy of the charge distribution. It may lead to double countings of the penetration effect for configurations where multipoles are already overestimated. Overall, on the 10 dimer configurations, the best choice is based on GDMA multipoles up to quadrupole fitted on atoms only and corrected by a damping function going up to the quadrupole level.

Besides the application to a SIBFA-like protocol, we also applied this methodology to treat charge penetration within the AMOEBA framework, which uses only atom centered ESP multipoles on various systems. As we discussed, ESP multipoles do take not full advantages of higher order penetration correction as the charge-dipole damping appears already weaker than in the case of well behaved multipoles.

In all these cases, we have significantly improved the AMOEBA results without modifying the existing sets of multipoles (amoeba09).

For the previously discussed water dimers, the maximum energy variation between the first six configurations, corresponding to the lowest energies, the charge-charge correction reproduced well the behavior of SAPT energy variations between configurations (energy difference between the most and the less stable configuration: 2.5 for SAPT) whereas other corrections appear strongly less anisotropic (0.9 kcal/mol for Ref. 25). Even for this simplest level of correction, penetration effects are well recovered. Indeed, Figure 4 represents the electrostatic energy between two water molecules as a function of their intermolecular distance in Angströms. The first two geometries (Figs. 4a and 4b) correspond to strong H-bonds while the third (Fig. 4c) involves two H-bonds and the fourth (Fig. 4d) weak interactions.

We also report the root mean square error for intermolecular distance scans (from 1.4 to 2.7 A) of selected water dimers (S66 is an additional water geometry extracted from S66 set) in Table 3 which confirms the improvement using AMOEBA model in different configurations and the robustness of the correction at very short range. The small improvement between the RMSE's regarding water dimer 7 (Fig. 4d) could be explained by its being a high lying energy dimer obtained only at the CCSDT level.[43] Indeed, for this kind of system, the charge penetration correction remains subtle because of the importance of electronic correlation and of the difficulty to model interaction involving the use of very diffuse basis function.

We continue our investigation on other chemical functions: methanol (MeOH) and methyl amine (MeNH2) (see Appendix Tables A1 and A2, respectively). Finally, we investigate again benzene (see Appendix Table 3 and 5). In all these cases, we improved the electrostatics using AMOEBA multipoles and particularly for benzene dimers. The approximation only breaks at very -unphysical- short-range. We report all our results in Figure 4, a plot of the results obtained with the correction against SAPT reference values. This graph includes all the presented molecules and their distance scans from near-equilibrium up to short distances (Fig. 5).

The electrostatic interaction energies of some of these complexes are for distances far below equilibrium and for these penetration effects can be very significant. As one can see from the Tables (Appendix), the penetration correction always improved the results compared with SAPT, even for the cases where ESP multipolar energies were really off (see benzene results), with the wrong interaction sign in all cases.

To conclude, we extended our tests to charged systems, studying complexes of water with the metal cations K^+, Na^+, Mg^{2+}, Ca^{2+}, and Zn^{2+} (Fig. 6).

As expected from the previous SIBFA work, penetration effects are a key element to model metal cations. The simple addition of the charge-charge correction enables a very close agreement with reference SAPT datas.

Parallel Implementation. The loops involved in the computation of the correction term can be easily parallelized with a shared memory (OPENMP), distributed memory (MPI) or hybrid (OPENMP/MPI) paradigm. The additional routines are included in a parallel version of the SPME that we developed in the upcoming Tinker-hp software[51–54]: the atom sites and the corresponding energies and forces are distributed among processes using a spatial decomposition. Furthermore, as the cutoff used in the correction term (between 6 and 8 Å) is usually smaller than the real space cutoff (see Fig. 2) used in the SPME, no additional cross-processor communication of the atomic positions between each time step is necessary. The parallel scaling of the computation of the correction using MPI is showed on graph 7 for a water box of 60 000 atoms in a cubic unit cell where each edge is 84 Å long. Our tests showed that a pure MPI implementation is faster than a hybrid one before reaching a scaling plateau, but once this plateau is reached, the hybrid implementation allows to make use of more cores and to improve the best timing. The best timings obtained to compute both the electrostatic forces using SPME, and the correction, using the pure MPI implementation are shown in Table 4, as well as the best timings obtained with the hybrid implementation (with 2 OpenMP threads per MPI process; Fig. 7).

With a cutoff of 8 Å, which is beyond convergence, the total penetration cost is only 25% in both cases. Of course, as we discussed, such a cutoff can be chosen more aggressively. A more aggressive cutoff of 4 angstroms symbol (see Fig. 2) captured 99% of penetration interaction and led to strong decrease of the computation cost which became lower than 10%.

Conclusions

We have studied the general coupling of an empirical short-range charge penetration correction to the SPME. The corrected SPME approach allows a computationally efficient and accurate improvement of electrostatics in polarizable

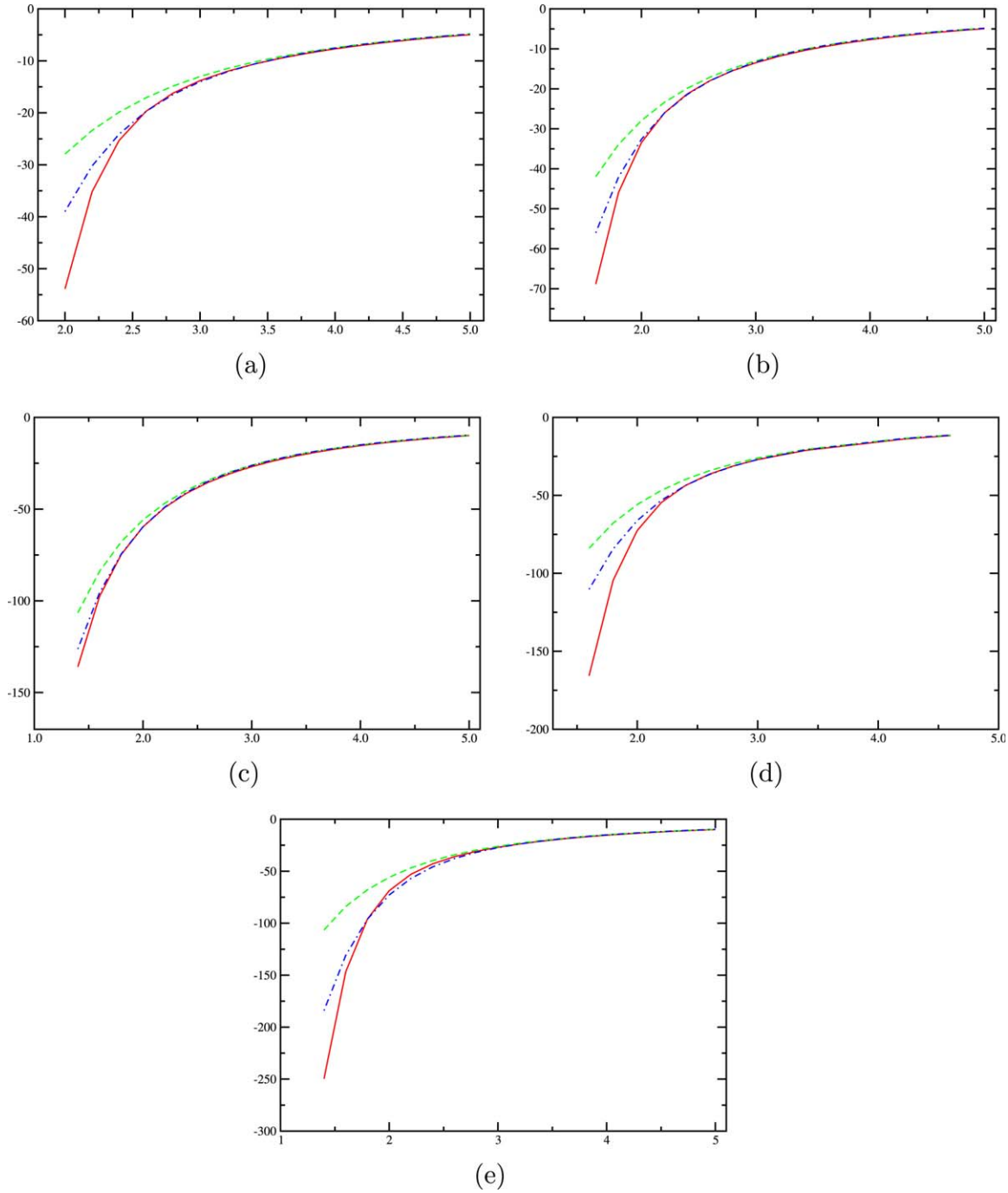

Figure 6. Cation-water complexes: electrostatic variation as function of cation-O distance in kcal/mol. SAPT is the red line, AMOEBA the green dashed line and the penetration correction blue dashed-dot line. a) K^+ water complex. b) Na^+ water complex. c) Mg^{2+} water complex. d) Ca^{2+} water complex. e) Zn^{2+} water complex. [Color figure can be viewed in the online issue, which is available at wileyonlinelibrary.com.]

simulations by correcting the short-range charge-charge, charge-dipole and charge-quadrupole terms. The method has been implemented in the TINKER-HP software and the additional cost of the short-range damping function shown to be small as the global electrostatics implementation exhibits a favorable parallel scaling at the MPI and OPEN-MP/MPI hybrid levels. A separate cutoff for the penetration term coupled to a switching function has been implemented to maintain the possibility of a performance optimization of SPME thanks to the separate Ewald cutoff. Initial tests have been performed in the context of the AMOEBA and SIBFA force fields (ESP and GDMA approaches, respectively). Substantial improvements were noted in the agreement of standard noncorrected multipolar interaction energies (from Stone multipoles[29]) compared with SAPT *ab-initio* reference data. As we discussed the effects of spurious fit of

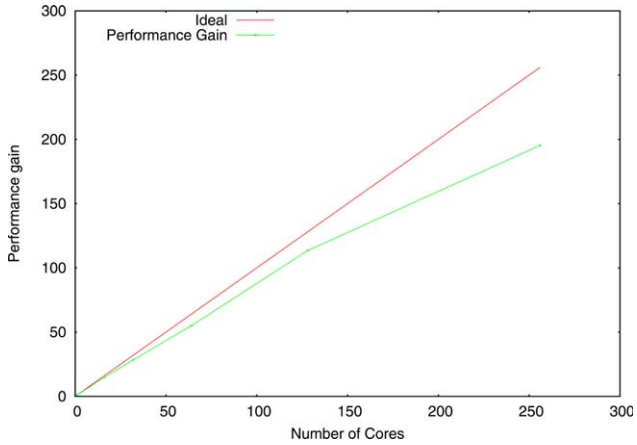

Figure 7. Parallel scaling for a water box of 60 000 atoms. [Color figure can be viewed in the online issue, which is available at wileyonlinelibrary.com.]

distributed multipoles, the need of comparing atom-centered GDMA to SAPT is highlighted as one wants to avoid overfitted multipolar energies. When the distributed moments are physically meaningful, the correction exhibits a systematic improvement when adding charge-charge, then charge-dipole and charge-quadrupole corrections. For some sets of multipoles, like the ESP one, that exhibit some fictitious inclusion of penetration the correction should be small to the charge-charge correction only. For these types of multipoles, specific parametrization procedure has been recently proposed in Ref. 55 based on ESP derivation of the damping parameters.

Finally, it is important to point out that, at the end, an error compensation between the damping function and the set of multipoles has to be found. Others damping function exist and will be studied to find the best agreement according to the different force field models (Rackers et al., in preparation).

This opens two possible strategies as one can focus on the sole optimization of the charge-charge term to obtain a significant improvement of atom centered multipolar electrostatics at a very low computational cost. Strategies in that direction are currently studied in the context of AMOEBA-like potentials.

A second strategy includes higher order damping corrections (charge dipole and beyond), as presented in the SIBFA potential. Such an implementation is therefore the starting point of SIBFA porting into Tinker-hp. Prospective applications in biochemistry, pharmacology and nuclear science[15,56–58] should benefit from the inclusion of charge penetration in PBC MD with improved representations of short-range contributions exchange-repulsion and charge transfer and long-range polarization and dispersion. To conclude, it is important to point out that future inclusion of such corrections in polarizable MD will require either to reparametrize the van der Waals contribution in the case of AMOEBA-like potentials or to use the penetration-corrected electrostatics in conjunction with an explicit exchange-repulsion contribution as in SIBFA.

APPENDIX A

Forces

$$\frac{\partial(E^*_{m_i-m_j}-E_{m_i-m_j})}{\partial r_i^\alpha}=\frac{(r_j-r_i)^\alpha}{r_{ij}^\alpha}(Z_i(Z_j-q_j)\exp(-\alpha_j r_{ij})(\alpha_j+\frac{1}{r_{ij}})$$
$$+Z_j(Z_i-q_i)\exp(-\alpha_i r_{ij})(\alpha_i+\frac{1}{r_{ij}})$$
$$+(Z_i-q_i)(Z_j-q_j)(\exp(-(\beta_i+\beta_j)r_{ij})(\beta_i+\beta_j+\frac{1}{r_{ij}})$$
$$-\exp(-\beta_i r_{ij})(\beta_i+\frac{1}{r_{ij}})-\exp(-\beta_j r_{ij})(\beta_j+\frac{1}{r_{ij}}))\tag{21}$$

$$\frac{\partial(E^*_{m_i-d_j}-E_{m_i-d_j})}{\partial r_i^\alpha}=\frac{(Z_i-q_i)\exp(-\eta r_{ij})}{r_{ij}^3}(\mu_j^\alpha+(r_j-r_i)^\alpha\frac{\mathbf{\mu}_j.\mathbf{r}_{ji}}{r_{ij}}(\eta+\frac{3}{r_{ij}}))\tag{22}$$

Torques

Because the energy correction term contains permanent dipole moments that are usually defined in local frames bound to neighboring atoms, the derivatives of this term with respect to the positions of these atoms have to be taken into account. These are often improperly refered to as "torques." Suppose that the k-th atom is used to define the local frame in which the dipole moment $\boldsymbol{\mu}_j$ is written, then the corresponding derivative is the following:

$$\frac{d(E^*_{m_i-d_j}-E_{m_i-d_j})}{dr_k^\alpha}=\frac{\partial(E^*_{m_i-d_j}-E_{m_i-d_j})}{\partial r_k^\alpha}+<\frac{\partial(E^*_{m_i-d_j}-E_{m_i-d_j})}{\partial\ \boldsymbol{\mu}_j},\frac{\partial\ \boldsymbol{\mu}_j}{\partial r_k^\alpha}>\tag{23}$$

$$\frac{d(E^*_{m_i-d_j}-E_{m_i-d_j})}{dr_k^\alpha}=\frac{\partial(E^*_{m_i-d_j}-E_{m_i-d_j})}{\partial r_k^\alpha}+<(Z_i-q_i)\exp(-\eta r_{ij})\frac{r_{ji}}{r_{ij}^3},\frac{\partial\ \boldsymbol{\mu}_j}{\partial r_k^\alpha}>\tag{24}$$

where the derivatives of $\boldsymbol{\mu}_j$ involve the derivatives of the derivatives of the rotation matrix used to go from the local to the global frame

Data

Tables A1 and A2 report electrostatics using two different distributed multipolar sites scheme: (i) atoms plus bonds (Table A1). (ii) atoms only (Table A2). Space Partitioning and hydrogen radii were also tested. sw*i*-rad*j* denotes the space partitioning choice (switch *i* in GDMA) and *j* is the hydrogen radius.

We have retained the S66 [47] dimer notations.

Acknowledgment

The authors wish to thank Marie-France Couret for technical support.

Table A1. Multipolar electrostatics using moments on bonds and atoms (values in kcal/mol).

Index	sw0-rad325	sw0-rad65	sw2-rad325	sw2-rad65	sw4-rad325	sw4-rad65
1	−6.18	−6.50	−6.91	−8.14	−6.96	−8.21
2	−5.19	−5.47	−5.22	−7.07	−5.23	−7.11
3	−5.05	−5.33	−4.88	−6.93	−4.88	−6.96
4	−5.13	−4.99	−4.72	−4.63	−4.69	−4.63
5	−4.51	−4.41	−3.55	−3.98	−3.48	−3.95
6	−4.32	−4.26	−3.19	−3.89	−3.11	−3.85
7	−3.59	−3.46	−3.51	−3.06	−3.50	−3.05
8	−1.04	−1.03	−1.27	−1.09	−1.28	−1.10
9	−3.32	−3.29	−3.87	−3.54	−3.89	−3.57
10	−1.96	−1.91	−2.24	−1.97	−2.25	−1.98

Table A2. Multipolar electrostatics using moments on atoms only (values in kcal/mol).

Index	sw0-rad325	sw0-rad65	sw2-rad325	sw2-rad65	sw4-rad325	sw4-rad65
1	−6.02	−6.54	−6.73	−7.94	−6.75	−7.93
2	−5.12	−5.51	−5.15	−6.92	−5.16	−6.90
3	−5.01	−5.36	−4.85	−6.80	−4.86	−6.77
4	−5.31	−5.01	−4.82	−4.66	−4.81	−4.68
5	−4.81	−4.44	−3.76	−4.05	−3.74	−4.04
6	−4.67	−4.28	−3.44	−3.96	−3.42	−3.95
7	−3.49	−3.44	−3.58	−3.08	−3.58	−3.09
8	−0.93	−1.04	−1.26	−1.10	−1.26	−1.11
9	−3.06	−3.28	−3.79	−3.53	−3.80	−3.56
10	−1.87	−1.92	−2.21	−2.00	−2.21	−2.02

Table A3. Multipolar electrostatics and penetration correction decomposed (energy values in kcal/mol).

SAPT	GDMA[1]	E_{pen}	E_{pen} charge-charge	E_{pen} charge-dipole	E_{pen} charge-quadrupole
−8.18	−6.73	−1.44	−1.22	−0.11	0.12
−6.64	−5.15	−1.48	−1.15	−0.14	0.20
−6.36	−4.85	−1.51	−1.14	−0.15	0.23
−6.58	−4.82	−1.76	−1.57	−0.03	0.15
−5.78	−3.76	−2.02	−1.65	−0.08	0.29
−5.58	−3.44	−2.14	−1.70	−0.10	0.34
−4.71	−3.58	−1.13	−1.13	0.03	0.03
−1.43	−1.26	−0.18	−0.25	0.04	−0.04
−4.84	−3.79	−1.04	−1.00	−0.03	0.02
−2.82	−2.21	−0.61	−0.58	−0.02	0.01

Table A4. CP-AMOEBA parameters.

Fragments	Atoms	α	β	η
Water	H	3.5	2.9	1.7
	O	4.0	4.9	4.7
	H(—H3C)	3.5	2.6	4.7
Methanol	C(—CH3)	5.8	4.9	2.5
	O	6.4	4.5	0.7
	H(—O)	4.8	2.9	1.7
Methylamine	H(—H3C)	3.5	2.7	4.7
	C(—CH3)	4.8	5.4	2.5
	N	4.8	4.8	2.7
	H(—N)	2.5	2.9	1.7
Benzene	C	2.8	2.5	2.8
	H	3.5	2.3	2.5

Table A5. Distance scans of S66 water orientations (energy values in kcal/mol).

Dimers	SAPT	AMOEBA	CP-AMOEBA
2699_01WaterWater090	−10.687	−7.469	−10.136
2700_01WaterWater095	−8.739	−6.407	−8.423
2701_01WaterWater100	−7.231	−5.542	−7.058
2702_01WaterWater105	−6.052	−4.826	−5.961
2703_01WaterWater110	−5.124	−4.230	−5.078

Table A6. Distance scans of various methanol dimer orientations (energy values in kcal/mol).

Dimers	SAPT	AMOEBA	CP-AMOEBA
2707_02WaterMeOH090	−12.337	−7.530	−12.656
2708_02WaterMeOH095	−10.053	−6.282	−10.124
2709_02WaterMeOH100	−8.280	−5.274	−8.180
2710_02WaterMeOH105	−6.891	−4.447	−6.667
2711_02WaterMeOH110	−5.799	−3.764	−5.480
2731_05MeOHMeOH090	−12.915	−6.222	−14.330
2732_05MeOHMeOH095	−10.488	−5.047	−11.082
2733_05MeOHMeOH100	−8.605	−4.096	−8.644
2734_05MeOHMeOH105	−7.133	−3.314	−6.788
2735_05MeOHMeOH110	−5.979	−2.667	−5.364
2755_08MeOHWater090	−11.037	−6.1497	−11.042
2756_08MeOHWater095	−8.991	−5.163	−8.815
2757_08MeOHWater100	−7.410	−4.356	−7.102
2758_08MeOHWater105	−6.177	−3.686	−5.770
2759_08MeOHWater110	−5.211	−3.128	−4.728

Table A7. Distance scans of various methylamine dimer orientations (energy values in kcal/mol).

Dimers	SAPT	AMOEBA	CP-AMOEBA
2715_03WaterMeNH2090	−16.578	−14.156	−16.557
2716_03WaterMeNH2095	−13.653	−12.178	−13.894
2717_03WaterMeNH2100	−11.328	−10.595	−1.817
2718_03WaterMeNH2105	−9.468	−9.311	−10.175
2719_03WaterMeNH2110	−7.978	−8.261	−8.867
2739_06MeOHMeNH2090	−18.216	−12.793	−18.129
2740_06MeOHMeNH2095	−14.938	−10.881	−14.790
2741_06MeOHMeNH2100	−12.337	−9.354	−12.240
2742_06MeOHMeNH2105	−10.262	−8.117	−10.267
2743_06MeOHMeNH2110	−8.605	−7.107	−8.727
2763_09MeNH2MeOH090	−6.139	−3.797	−2.151
2764_09MeNH2MeOH095	−4.758	−3.364	−2.177
2765_09MeNH2MeOH100	−3.748	−3.011	−2.172
2766_09MeNH2MeOH105	−3.002	−2.719	−2.145
2767_09MeNH2MeOH110	−2.444	−2.475	−2.101
2771_10MeNH2MeNH2090	−9.181	−7.864	−6.372
2772_10MeNH2MeNH2095	−7.163	−7.199	−6.048
2773_10MeNH2MeNH2100	−5.661	−6.655	−5.761
2774_10MeNH2MeNH2105	−4.530	−6.207	−5.505
2775_10MeNH2MeNH2110	−3.675	−5.835	−5.278
2787_12MeNH2Water090	−17.110	−13.859	−17.396
2788_12MeNH2Water095	−14.075	−11.953	−14.576
2789_12MeNH2Water100	−11.665	−10.426	−12.369
2790_12MeNH2Water105	−9.740	−9.185	−10.621
2791_12MeNH2Water110	−8.201	−8.169	−9.226

Table A8. Distance scans of benzene water values (energy values in kcal/mol).

Dimers	SAPT	AMOEBA	CP-AMOEBA
3123_54BenzeneWaterOHpi090	−4.370	5.499	−5.296
3124_54BenzeneWaterOHpi095	−3.432	5.486	−3.795
3125_54BenzeneWaterOHpi100	−2.769	5.536	−2.668
3126_54BenzeneWaterOHpi105	−2.288	5.620	−1.815
3127_54BenzeneWaterOHpi110	−1.932	5.721	−1.166

Table A9. Distance scan of benzene π stacking (energy values in kcal/mol).

Dimers	SAPT	AMOEBA	CP-AMOEBA
2883_24BenzeneBenzenepipi090	−8.480	15.690	−11.851
2884_24BenzeneBenzenepipi095	−4.749	15.556	−6.321
2885_24BenzeneBenzenepipi100	−2.564	15.430	−2.743
2886_24BenzeneBenzenepipi105	−1.292	15.314	−0.428
2887_24BenzeneBenzenepipi110	−0.560	15.208	1.639

Table A10. Benzene T-shaped (energy values in kcal/mol).

Dimers	SAPT	AMOEBA	CP-AMOEBA
3067_47BenzeneBenzeneTS090	−4.928	13.934	−13.167
3068_47BenzeneBenzeneTS095	−3.224	13.936	−8.150
3069_47BenzeneBenzeneTS100	−2.160	13.956	−4.706
3070_47BenzeneBenzeneTS105	−1.486	13.985	−2.324
3071_47BenzeneBenzeneTS110	−1.055	14.018	−0.673

Keywords: polarizable force fields · electrostatics · energy decomposition analysis

How to cite this article: C. Narth, L. Lagardère, É. Polack, N. Gresh, Q. Wang, D. R. Bell, J. A. Rackers, J. W. Ponder, P. Y. Ren, J.-P. Piquemal *J. Comput. Chem.* **2016**, *37*, 494–505. DOI: 10.1002/jcc.24257

[1] F. H. Allen, *Acta Crystallogr. Sect. B* **2002**, *58*, 380.
[2] F. C. Bernstein, T. F. Koetzle, G. J. Williams, E. F. Meyer, Jr, M. D. Brice, J. R. Rodgers, O. Kennard, T. Shimanouchi, M. Tasumi, *Arch. Biochem. Biophys.* **1978**, *185*, 584.
[3] UniProt Consortium, *Nucleic Acids Res.* **2014**, *42*, D191.
[4] H. Lodish, A. Berk, S. L. Zipursky, et al. Molecular Cell Biology, 4th ed. W. H. Freeman: New York, **2000**. Available from: http://www.ncbi.nlm.nih.gov/books/NBK21475/.
[5] C. W. Pratt, D. Voet, J. G. Voet, Fundamentals of biochemistry: life at the molecular level; Wiley: New York, **2005**.
[6] L. V. Slipchenko, M. S. Gordon, *Mol. Phys.* **2009**, *107*, 999.
[7] J. P. Piquemal, N. Gresh, C. Giessner-Prettre, *J. Phys. Chem. A* **2003**, *107*, 10353.
[8] C. M. Handley, P. L. Popelier, *J. Phys. Chem. A* **2010**, *114*, 3371.
[9] D. M. Elking, G. A. Cisneros, J. P. Piquemal, T. A. Darden, L. G. Pedersen, *J. Chem. Theory Comput.* **2009**, *6*, 190.
[10] R. Chaudret, N. Gresh, C. Narth, L. Lagardère, T. A. Darden, G. A. Cisneros, J.-P. Piquemal, *J. Phys. Chem. A* **2014**, *118*, 7598.
[11] T. J. Giese, H. Chen, T. Dissanayake, G. M. Giambaşu, H. Heldenbrand, M. Huang, E. R. Kuechler, T. S. Lee, M. T. Panteva, B. K. Radak, D. M. York, *J. Chem. Theory Comput.* **2013**, *9*, 1417.
[12] U. Essmann, L. Perera, M. L. Berkowitz, T. Darden, H. Lee, L. G. Pedersen, *J. Chem. Phys.* **1995**, *103*, 8577.
[13] T. Darden, D. York, L. Pedersen, *J. Chem. Phys.* **1993**, *98*, 10089.
[14] P. Ren, C. Wu, J. W. Ponder, *J. Chem. Theory Comput.* **2011**, *7*, 3143.
[15] N. Gresh, G. A. Cisneros, T. A. Darden, J. P. Piquemal, *J. Chem. Theory Comput.* **2007**, *3*, 1960.
[16] N. Gresh, P. Claverie, A. Pullman, *Theor. Chim. Acta* **1984**, *66*, 1.
[17] J. P. Piquemal, B. Williams-Hubbard, N. Fey, R. J. Deeth, N. Gresh, C. Giessner-Prettre, *J. Comput. Chem.* **2003**, *24*, 1963.
[18] J. P. Piquemal, H. Chevreau, N. Gresh, *J. Chem. Theory Comput.* **2007**, *3*, 824.
[19] M. Devereux, N. Gresh, J. P. Piquemal, M. Meuwly, *J. Comput. Chem.* **2014**, *35*, 1577.
[20] G. Cisneros, S. Tholander, O. Parisel, T. Darden, D. Elking, L. Perera, J. P. Piquemal, *Int. J. Quantum Chem.* **2008**, *108*, 1905.
[21] A. S. Werneck, T. M. R. Filho, L. E. Dardenne, *J. Phys. Chem. A* **2008**, *112*, 268.
[22] J. P. Piquemal, G. A. Cisneros, P. Reinhardt, N. Gresh, T. A. Darden, *J. Chem. Phys.* **2006**, *124*, 104101.
[23] M. A. Freitag, M. S. Gordon, J. H. Jensen, W. Stevens, *J. J. Chem. Phys.* **2000**, *112*, 7300.
[24] A. Stone, *J. Phys. Chem. A* **2011**, *115*, 7017.
[25] B. Wang, D. G. Truhlar, *J. Chem. Theory Comput.* **2014**, *10*, 4480.
[26] F. A. Momany, *J. Phys. Chem.* **1978**, *82*, 592.
[27] G. A. Cisneros, M. Karttunen, P. Ren, C. Sagui, *Chem. Rev.* **2013**, *114*, 779.
[28] R. J. Wheatley, J. B. Mitchell, *J. Comput. Chem.* **1994**, *15*, 1187.
[29] A. Stone, *Chem. Phys. Lett.* **1981**, *83*, 233.
[30] F. Vigné-Maeder, P. Claverie, *J. Chem. Phys.* **1988**, *88*, 4934.
[31] Claverie, P. Contribution à l'étude des interactions intermoléculaires. Ph.D. thesis, UPMC, **1973**.
[32] E. G. Hohenstein, J. Duan, C. D. Sherrill, *J. Am. Chem. Soc.* **2011**, *133*, 13244.
[33] M. Jeziorska, W. Cencek, K. Patkowski, B. Jeziorski, K. Szalewicz, *J. Chem. Phys.* **2007**, *127*, 124303.
[34] B. Jeziorski, R. Moszynski, K. Szalewicz, *Chem. Rev.* **1994**, *94*, 1887.
[35] P. P. Ewald, *Ann. Der Phys.* **1921**, *369*, 253.
[36] J. W. Perram, H. G. Petersen, S. W. De Leeuw, *Mol. Phys.* **1988**, *65*, 875.
[37] C. Sagui, L. G. Pedersen, T. A. Darden, *J. Chem. Phys.* **2004**, *120*, 73.
[38] E. R. Smith, *Proc. R. Soc. London A* **1981**, *375*, 475.
[39] W. Smith, *Inf. Newslett. Comput. Simul. Condens. Phases* **1998**, 15.
[40] J. Norberg, L. Nilsson, *Biophys. J.* **2000**, *79*, 1537.
[41] B. R. Brooks, R. E. Bruccoleri, B. D. Olafson, D. J. States, S. Swaminathan, M. Karplus, *J. Comput. Chem.* **1983**, *4*, 187.
[42] R. J. Loncharich, B. R. Brooks, *Proteins: Struct. Funct. Bioinformatics* **1989**, *6*, 32.
[43] P. Reinhardt, J. P. Piquemal, *Int. J. Quantum Chem.* **2009**, *109*, 3259.
[44] J. van Duijneveldt-van de Rijdt, W. Mooij, F. van Duijneveldt, *Phys. Chem. Chem. Phys.* **2003**, *5*, 1169.
[45] B. J. Smith, D. J. Swanton, J. A. Pople, I. I. I. Schaefer, H. F. Radom, *J. Chem. Phys.* **1990**, *92*, 1240.
[46] G. S. Tschumper, M. L. Leininger, B. C. Hoffman, E. F. Valeev, H. F. Schaefer III, Quack, *J. Chem. Phys.* **2002**, *116*, 690.
[47] J. Rezác, K. E. Riley, P. Hobza, *J. Chem. Theory Comput.* **2011**, *7*, 2427.
[48] L. Goerigk, H. Kruse, S. Grimme, *ChemPhysChem* **2011**, *12*, 3421.
[49] W. J. Stevens, W. H. Fink, *Chem. Phys. Lett.* **1987**, *139*, 15.
[50] J. M. Turney, A. C. Simmonett, R. M. Parrish, E. G. Hohenstein, F. A. Evangelista, J. T. Fermann, B. J. Mintz, L. A. Burns, J. J. Wilke, M. L. Abrams, *Wiley Interdiscip. Rev.: Comput. Mol. Sci.* **2012**, *2*, 556.
[51] F. Lipparini, B. Stamm, E. Cancès, Y. Maday, B. Mennucci, *J. Chem. Theory Comput.* **2013**, *9*, 3637.
[52] F. Lipparini, G. Scalmani, L. Lagardère, B. Stamm, E. Cancès, Y. Maday, J. P. Piquemal, M. J. Frisch, B. Mennucci, *J. Chem. Phys.* **2014**, *141*, 184108.
[53] F. Lipparini, L. Lagardère, B. Stamm, E. Cancès, M. Schnieders, P. Ren, Y. Maday, J. P. Piquemal, *J. Chem. Theory Comput.* **2014**, *10*, 1638.
[54] L. Lagardère, F. Lipparini, B. Stamm, E. Cancès, M. Schnieders, P. Ren, Y. Maday, J.-P. Piquemal, Submitted.
[55] Q. Wang, J. A. Rackers, C. He, R. Qi, C. Narth, L. Lagardere, N. Gresh, J. W. Ponder, J. P. Piquemal, P. Ren, *J. Chem. Theory Comput.* **2015**, *11*, 2609.
[56] J. C. Wu, J. P. Piquemal, R. Chaudret, P. Reinhardt, P. Ren, *J. Chem. Theory Comput.* **2010**, *6*, 2059.
[57] J. Zhang, W. Yang, J. P. Piquemal, P. Ren, *J. Chem. Theory Comput.* **2012**, *8*, 1314.
[58] A. Marjolin, C. Gourlaouen, C. Clavaguéra, P. Y. Ren, J. P. Piquemal, J. P. Dognon, *J. Mol. Model.* **2014**, *20*, 1.

Received: 25 March 2015
Revised: 2 August 2015
Accepted: 21 October 2015
Published online in Wiley Online Library